Pergamon

Acta Materialia 50 (2002) 619–631

Acta MATERIALIA

www.elsevier.com/locate/actamat

First-principles study of metal–carbide/nitride adhesion: Al/VC vs. Al/VN

Donald J. Siegel [a,*], Louis G. Hector Jr. [b,1], James B. Adams [c,2]

[a] *Department of Physics, University of Illinois at Urbana–Champaign, 1110 West Green Street, Urbana, IL 61801, USA*
[b] *Surface Science Division, ALCOA Technical Center, ALCOA Center, PA 15069-0001, USA*
[c] *Chemical and Materials Enigneering Department, Arizona State University, Tempe, AZ 85287-6006, USA*

Received 7 August 2001; accepted 31 August 2001

Abstract

We have performed density functional calculations to investigate the adhesion and electronic structure at interfaces between Al and the refractory transition metal nitrides/carbides VN and VC in order to understand the significance of the ceramic's metalloid component upon interfacial properties. We find that for both systems the preferred bonding site places the metal interfacial atoms above the ceramic's metalloid atoms, and that adhesion energies are comparable to those found for other metals (Ti, Ag) on MgO. The differences in magnitude and rank-ordering of the adhesion energies for the two interfaces are rationalized in terms of the the surface energies of the ceramics. Analysis of the charge density and density of states reveals that covalent Al–C/N bonds constitute the dominant metal–ceramic interaction.

Keywords: Ab initio calculation; Aluminum; Carbides; Interfacial adhesion; Nitrides

1. Introduction

Interfaces between metals and ceramics play a vital role in many industrial applications [1]: heterogeneous catalysis, microelectronics, thermal barriers, corrosion protection and metals processing are but a few representative examples. However, experimental complications associated with the study of a buried interface, and theoretical difficulties arising from complex interfacial bonding interactions, have hindered the development of general, analytic models capable of accurately predicting fundamental interfacial quantities.

One such quantity that is key to predicting the mechanical properties of an interface is the ideal work of adhesion, $\mathscr{W}_{ad}$ [1], which is defined as the bond energy needed (per unit area) to reversibly separate an interface into two free surfaces, neglecting plastic and diffusional degrees of freedom. For example, the degree of plastic deformation that occurs during interfacial fracture is known to

* Corresponding author. Present address: Thin Film and Interface Science Group, Sandia National Laboratories, Mail Stop 9161, Livermore, CA 94551-0969, USA. Tel.: 925-294-3089; fax: 925-294-3231.
E-mail address: djsiege@sandia.gov (D.J. Siegel).
[1] Present address: General Motors R&D Center , Mail Code 480-106-224, 30500 Mound Rd, Warren, MI 48090-9055, USA.
[2] Visit http://ceaspub.eas.asu.edu/cms.

1359-6454/02/$22.00
PII: S1359-6454(01)00361-5

depend upon $\mathscr{W}_{ad}$ [2–4]. Formally, $\mathscr{W}_{ad}$ can be defined in terms of either the surface and interfacial energies (relative to the respective bulk materials) or by the difference in total energy between the interface and its isolated surfaces:

$$\mathscr{W}_{ad} = \sigma_{1v} + \sigma_{2v} - \gamma_{12} = (E_1^{tot} + E_2^{tot} - E_{12}^{tot})/A. \quad (1)$$

Here, σ_{iv} is the surface energy of slab i, γ_{12} is the interface energy, E_i^{tot} is the total energy of slab i and E_{12}^{tot} is the total energy of the interface system. The total interface area is given by A.

Although there has recently been much activity aimed at understanding metal/oxide interfaces [1,5–12], much less is known about metal/ceramic adhesion involving non-oxide ceramics. Within this class, the transition metal carbides and nitrides are a particularly notable omission, considering their exceptional hardness, strength and corrosion resistance [13]. To our knowledge, there have been only three studies [14–16] of adhesion between metals and transition metal carbides/nitrides based on density functional theory (DFT) [17,18], along with a few earlier studies [19–21] performed using semi-empirical methods. Recently, our group examined the stability, $\mathscr{W}_{ad}$ and electronic structure of the polar Al(111)/WC(0001) interface [14], considering both C and W terminations of the ceramic. We determined that although the W-terminated interface had the lowest free energy, and was therefore more stable, the C termination had the largest $\mathscr{W}_{ad}$ of 6.0 J/m^2. Hartford [15] calculated the interfacial free energy of the Fe/VN system, including the effects of N vacancies. The interface energy was found to be negative for all systems consisting of more than one VN layer, with the presence of vacancies resulting in a small increase in interfacial energy. The interfacial bonds were determined to consist mainly of covalent N(p)–Fe(d) σ interactions, with minor V(d)–Fe(d) character. Finally, Dudiy and co-workers [16] examined the Co/TiC interface, and found that their calculated $\mathscr{W}_{ad}$ values agreed with wetting experiments to within 10%. The dominant bonding mechanism involved strong "metal-modified" covalent Co–C bonds.

Two groups have used DFT to study interfaces of Al with other non-oxide ceramics. Hoekstra and Kohyama [22] considered the polar Al/β-SiC(001) interface, and found relatively large adhesion energies of 6.42 and 3.74 J/m^2 for C and Si terminations, respectively. Conversely, a relatively weak adhesion of about 0.9 J/m^2 was found for the Al/AlN system by Ogata and Kitagawa [23]. On the experimental side, several groups (see Ref. [24] for a recent review) have investigated the wettability of ceramic substrates by various metals. The wettability of VN and VC has been examined for a few interfaces involving transition metals [25,26]; however, data pertaining to interfaces with Al are lacking.

In this work we present a theoretical comparison of metal/ceramic adhesion between Al/VN and Al/VC. Vanadium nitride/carbide, along with other refractory compounds, are commonly used in tribological applications as a wear-resistant coating for the purpose of reducing adhesion [27]. However, the factors that determine the adhesive properties of a given coating are still poorly understood, and evaluation of many coatings is often performed on a trial-and-error basis. At the other extreme, in microelectonics packaging there is generally a need for strong adhesion between a carbide/nitride layer and a metallic interconnect or SiO_2. Since the mechanical properties of an interface depend sensitively upon the detailed atomic and electronic structure at the junction, knowledge of this type would be a valuable tool in optimizing the performance of these, and other, systems.

The goal of this study is to calculate the electronic structure, $\mathscr{W}_{ad}$ and optimal geometries of the Al/VN and Al/VC interfaces within a first-principles framework in order to better understand the nature of metal/ceramic adhesion. Previous studies have shown this approach to be reliable in reproducing $\mathscr{W}_{ad}$ values from experiment [1,7,8,16]. The Al/VN and Al/VC system serves as a convenient model of simple metal/transition metal carbide/nitride adhesion, since moderately sized simulation cells may be used as a result of similar lattice geometries. Our emphasis here is on drawing comparisons between the effects of the non-metallic (metalloid) part of the carbide/nitride on adhesion. In particular, we would like to understand how the substitution VN→VC manifests itself in $\mathscr{W}_{ad}$ and to

explain any differences by analyzing the electronic structure of the interface.

The remainder of this paper is organized as follows. Section 2 describes the computational methodology used in this study. Section 3 presents the results of our bulk and surface calculations on the pure materials. The major results of this paper are presented in Section 4, where we discuss the adhesion, geometry and electronic structure of the Al/VN and Al/VC metal/ceramic interfaces. Finally, we summarize our findings in Section 5.

2. Methodology

For this study we employ density functional theory (DFT) [17,18], as implemented in the Vienna ab initio Simulation Package (VASP) [28]. VASP uses a plane-wave basis set for the expansion of the single-particle Kohn–Sham wavefunctions, and pseudopotentials [29,30] to describe the computationally expensive electron–ion interaction. (Additional information regarding the details of the pseudopotential implementation are provided in Section 3.) The ground-state charge density and energy are calculated using a pre-conditioned conjugate gradient minimization algorithm [31,32] coupled with a Pulay-like mixing scheme [33–35]. Sampling of the irreducible wedge of the Brillouin zone is performed with a regular Monkhorst–Pack grid of special **k**-points [36]. Due to numerical instabilities associated with integrating the step-function character of the 0 K Fermi–Dirac distribution, partial occupancies of the single-particle wavefunctions are introduced [37,38] with an energy level broadening of 0.1 eV. Ground-state atomic geometries were obtained by minimizing the Hellman–Feynman forces [39,40] using either a conjugate gradient [31] or a quasi-Newton [33] algorithm. Finally, the generalized gradient approximation (GGA) of Perdew and Wang [41] (PW91) was employed for evaluation of the exchange-correlation energy. More detailed descriptions of VASP can be found elsewhere [28].

Due to the substantial computational cost of performing a DFT calculation on supercells containing first row and transition metal elements, we emphasize that our molecular statics (0 K) predictions of structure and adhesion energies do not account for temperature and larger-scale size effects such as reconstructions and lattice mismatch. In addition, our models of VN and VC are restricted to perfect 1:1 V:N/C stoichiometry (to permit the use of smaller supercells), even though it is well known that carbides/nitrides of the Vb subgroup may contain 10–20% vacancies in the metalloid sublattice [13].

3. Bulk and surface calculations

3.1. Bulk properties

To assess the accuracy of the pseudopotential approximation we have performed a series of calculations on the bulk Al, VN and VC phases. Results for Al were presented in an earlier study [7] of the Al/α-Al_2O_3 interface, where it was shown that the lattice constant, bulk modulus and cohesive energy obtained with a norm-conserving RRKJ-type [29] GGA pseudopotential were in good agreement with experimental and other first-principles calculations.

Many transition metal mono-nitrides/carbides, including VN and VC, crystallize in the NaCl (rocksalt) structure. In order to gage the significance of the V 3*p* semi-core states on the bulk structural and electronic properties, we have performed comparison calculations on both materials using ultrasoft-type [30,48] (US) (in which the *p* states are treated only via partial-core corrections [49]) and "all-electron" projector augmented wave (PAW) pseudopotentials [50,51].

For the US pseudopotentials set, the V pseudopotential was generated with an atomic valence configuration of $3d^4 4s^1$, which is the ground state as predicted by DFT. The outermost cut-off radius, r_c, was set at 1.36 Å and the local potential was taken as the unscreened all-electron potential outside a radius, $r_{loc} = 1.78$ Å. The C and N US pseudopotentials were implemented with valence configurations of $2s^2 2p^2$ and $2s^2 2p^3$, respectively, while using the *d* channel as the local pseudopotential component. Cut-off radii were set to $r_c^N = 0.87$ Å and $r_c^C = 0.96$ Å. Partial core corrections are generally unnecessary for first row

elements, and therefore were not included for the metalloid elements.

The PAW pseudopotential set used a $3p^6d^4 4s^1$ valence configuration for V, with $r_{loc} = 0.94$ Å and $r_c = 1.22$ Å. The C and N pseudopotentials used the same valence configuration and local component as their US counterparts, while setting smaller $r_c^C = r_c^N = 0.79$ Å. More information regarding the VASP pseudopotentials database can be found in the literature [30,51].

Before starting the bulk calculations, the total energies of each unit cell were carefully checked for convergence with respect to **k**-points and plane-wave cut-off energy; it was found that 56 **k**-points were sufficient to ensure convergence to ~1–2 meV/atom for both VN and VC. To achieve the same level of accuracy with respect to basis set size, different plane-wave cut-off energies were required depending on which pseudopotential set was used: 350 (400) eV for US (PAW) VN, 290 (400) eV for US (PAW) VC. Table 1 compares our results for the lattice constants, bulk modulus and cohesive energy with those of experiment [44,45,47] and other first-principles calculations [15,42,43,46]. (There is some uncertainty in the experimental data [47] for the bulk modulus due to the presence of pores and undetected impurities in the samples. These values are indicated with parentheses in Table 1.) We find that, for both VN and VC, use of the PAW results in only minor changes to the US values, with both pseudopotential sets giving good agreement with the experimental lattice constant and cohesive energy. The trend in switching from US to PAW pseudopotentials is to produce slightly smaller lattice constants and bulk moduli, with larger cohesive energies. In the case of VN, agreement with the other all-electron full-potential linearized augmented plane-wave (FPLAPW) GGA values [42] and another calculation based on US pseudopotentials [15] is also very good. For VC, the only other *ab initio* calculations [43,46] available for comparison are based on the local density approximation (LDA) [52]. While our GGA calculations compare well

Table 1
Comparison of VN and VC bulk properties as calculated using different *ab initio* methods with experiment. Results for the present study are given in the first two rows for each material. Abbreviations for the pseudopotential methods are defined as follows: US, ultrasoft pseudopotentials; PAW, projector augmented wave pseudopotentials; NC, norm-conserving pseudopotentials

System	Method	a (Å)	B_0 (GPa)	E_{coh} (eV)
VN	GGA, US	4.132	316	12.21
	GGA, PAW	4.127	310	12.86
	GGA, FPLAPW[a]	4.12	333	–
	GGA, US[b]	4.13	317	–
	LDA, FPLAPW[a]	4.06	376	–
	LDA, NC[c]	4.19	338	–
	Experiment	4.126[d]	(233)[h]	12.49[e]
VC	GGA, US	4.170	304	13.86
	GGA, PAW	4.163	293	14.4
	LDA, NC[c]	4.22	321	–
	LDA, LMTO–ASA[f]	4.137	298	–
	Experiment	4.172[g]	(303)[h]	13.88[e]

[a] Ref. [42].
[b] Ref. [15].
[c] Ref. [43].
[d] $VN_{0.98}$ at 93 K, Ref. [44].
[e] Ref. [45].
[f] Ref. [46].
[g] $VC_{0.88}$ at 288 K, Ref. [44].
[h] Ref. [47].

with these in predicting the bulk modulus, the GGA lattice constants are in better agreement with experiment.

As a second, and perhaps more rigorous pseudopotential comparison, Fig. 1 shows the VN band structure evaluated using both US and PAW pseudopotentials at their respective lattice constants. The two methods agree very well for the occupied states (to within the plot resolution of the band lines), although there is some minor deviation for the higher-lying unoccupied bands. Similar agreement was obtained for the US and PAW VC band structures. We further note that our VN band structure agrees well with another recent all-electron FPLAPW calculation performed by Stampfl and co-workers [42].

Since the PAW is more computationally expensive, and since our tests show little — if any — loss of accuracy upon using the US pseudopotentials, we used the US pseudopotentials for the remainder of this work.

Although the electronic structure of the bulk phases of many transition metal mono-nitrides/carbides has been analyzed extensively via first-principles methods by other groups (see Refs. [42,53] and references therein), we present here a brief review of these properties in order to facilitate discussion of the interfacial electronic properties. Generally, the bonding in VN/VC can be classified as a combination of metallic, ionic and covalent, with the V *d* band being split into bonding and anti-bonding states by the octahedral crystal field of the metalloid atoms. Overall, these two materials share many features of their respective electronic structures despite having different numbers of electrons per unit cell. This so-called "rigid band" behavior manifests itself as an upward shift in the Fermi energy of VN with respect to VC (see Fig. 2) as more anti-bonding states are filled by the one additional electron per unit cell provided by the N atom. Consequently, VN is observed to have a smaller cohesive energy.

The metallic nature of the bonding can be attributed to the partially filled *d* bands, as evident in

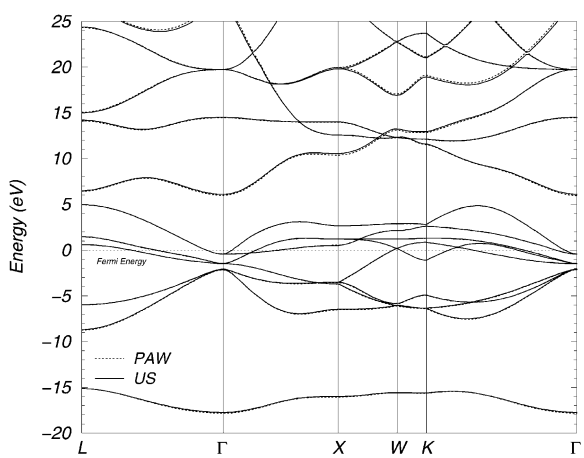

Fig. 1. Comparison of VN band structure as calculated using ultrasoft (solid lines) and PAW (dotted lines) pseudopotentials.

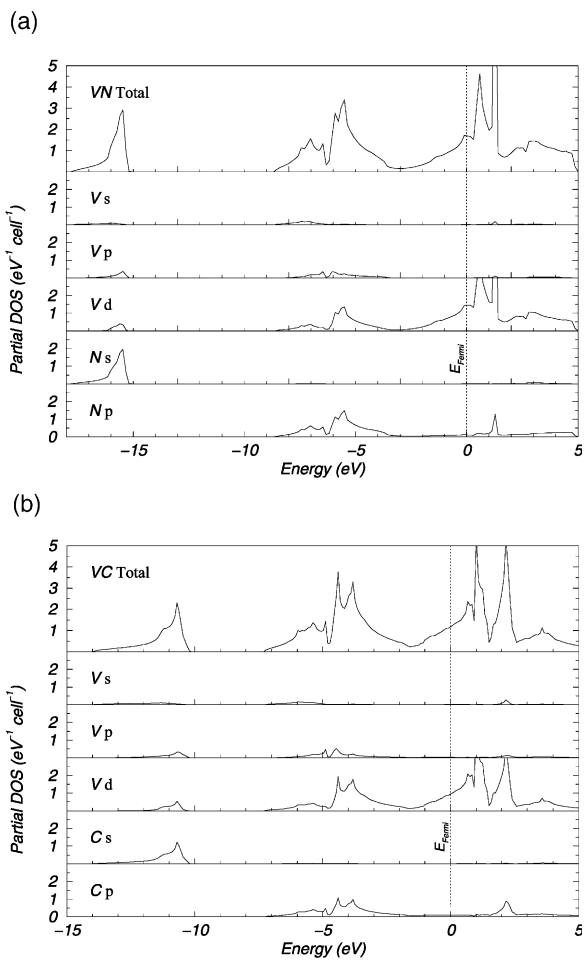

Fig. 2. Total and angular-momentum-projected DOS for bulk VN and VC. (a) VN; (b) VC.

the band structure (Fig. 1) or, more readily, by the peak in the partial density of states[3] (pDOS) near the Fermi energy (Fig. 2). The ionic nature of the V–metalloid bond is most clearly revealed in Fig. 3, as a substantial amount of charge density centered on the V atoms is transferred to the metalloid atoms upon formation of the compound. Moreover, the nearly spherically symmetric shape of the nitride difference charge suggests a larger ionic effect than in the carbide, which is consistent with the larger electronegativity of N. (However, the effects of ionicity appear to be less important than the filling of covalent anti-bonding states, as the cohesive energies do not correlate with the electronegativity of the metalloid.) Lastly, the presence of a covalent p–d σ interaction is indicated by the similar energy position and shape of the pDOS (Fig. 2) for the N/C p and V d states.

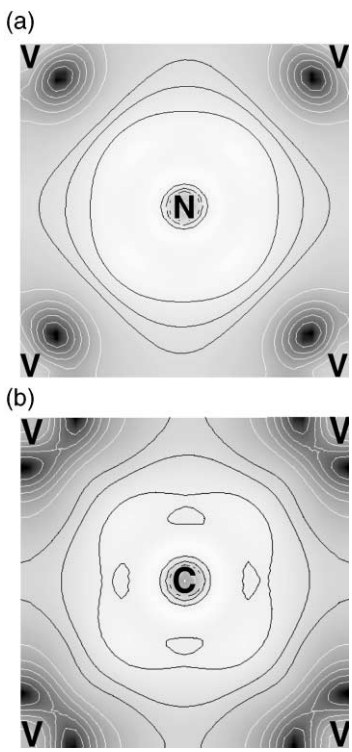

Fig. 3. Bulk VN and VC difference charge density (relative to the isolated atoms) through a (100) slice intersecting both V and N/C atoms. Charge redistribution is visualized by a gray-scale scheme in which lighter shades (black contour lines) indicate charge accumulation and darker shades (white contours) indicate charge depletion. (a) VN; (b) VC.

[3] The Wigner–Seitz radii for evaluation of the angular-momentum-projected DOS were set at: $r_V^{VN} = 1.51$ Å, $r_V^{VC} = 1.52$ Å, $r_C = 0.93$ Å and $r_N = 0.92$ Å. For Al we used $r_{Al} = 1.51$ Å.

3.2. Surface properties

The purpose of this study is to simulate the interface between two *bulk-like* slabs. It is therefore important to ensure that the slabs are sufficiently thick so as to exhibit bulk-like interiors, as it is known that the adhesion properties of thin films can differ significantly from those of thicker structures. To these ends, we have conducted convergence tests on the Al(100), VN(100) and VC(100) slabs in preparation for their use in interface calculations.

One way to ensure the presence of a bulk-like slab is to check for convergence of the surface energy with respect to the number of atomic layers, n. Upon attaining a critical thickness, the surface energy will converge to a fixed value, indicating that the two surfaces are decoupled by an intervening bulk region. We have calculated the surface energy for each of the (100) faces of Al, VN and VC for slabs of size ranging from three to 11 layers using the method proposed by Boettger [54] (see Table 2). Before doing so, a separate **k**-points test was performed on each surface supercell; to converge the total energy per atom to ~1–2 meV, the carbide/nitride surfaces required a set of 10 **k**-points, while for the Al system 36 **k**-points were sufficient. All structures were relaxed to a force

Table 2
Convergence of the surface energy with respect to slab thickness

Number of layers, n	Surface energy (J/m^2)		
	Al(100)	VN(100)	VC(100)
3	0.90	1.11	1.30
5	0.89	0.97	1.32
7	0.85	0.97	1.27
9	0.89	0.95	1.29
11	–	0.95	1.27

tolerance of 0.05 eV/Å per atom, and a 10 Å vacuum region was used to prevent interactions between periodic images.

As can be seen in Table 2, the surface energy for all three materials converges rapidly with increasing slab thickness to within about 0.05 J/m^2 for slabs with $n \geq 5$. An earlier study [7] on the Al/α-Al_2O_3 interface also observed rapid convergence for an Al(111) slab, where five layers were found to be sufficiently accurate for interface work. In that case a surface energy of 0.81 J/m^2 was measured, which is consistent with the present value of 0.89 J/m^2, as the close-packed (111) face of Al should exhibit a smaller surface energy than other low-index surfaces. We further note that the present value of the Al(100) surface energy is in good agreement with the experimental value [55,56] of 0.94 J/m^2, as extrapolated to 0 K. We are not aware of any reliable experimental data for the surface energies of VN or VC. Nonetheless, it is reasonable that the surface energy of VC (1.27 J/m^2) should be greater than that of VN (0.95 J/m^2) considering that VC has a larger cohesive energy.

In addition to our examination of the surface energy, we considered the surface relaxations as a function of slab thickness. We found that these were also well converged by five- to seven-layer slabs, with all relaxations being a relatively small 2% or less of the corresponding bulk spacings. For the VN and VC surfaces we refer here to the *average* relaxations, as there is some degree of surface rumpling present. In particular, while as a whole the first interlayer spacing in VN contracts by 1.7%, the individual V atoms relax inwards by 0.17 Å and the N atoms relax outwards by 0.1 Å. In VC the relaxations are smaller: the first interlayer spacing contracts by 1.4%, the V atom moves inwards by 0.09 Å and the C atom shifts outward by the same amount, 0.09 Å. For Al(100) the first interlayer spacing increases by 2%.

Based on the good convergence of the surface energies and relaxations, we conclude that slabs with $n \geq 5$ are sufficient for use in interface studies.

4. Interfaces

4.1. Model geometry

Our model of the Al/VN and Al/VC interfaces uses a superlattice geometry in which a seven-layer VN (or VC) (100) slab is placed between two five-layer slabs of Al(100), resulting in two identical interfaces per supercell with 24 total atoms. The free surfaces of the Al are separated by 10 Å of vacuum, and additional **k**-point tests showed that 28 sampling points were necessary to converge the total energy of the interface system to ~1–2 eV/atom. In addition to interfacing the (100) planes, the slabs were oriented about an axis normal to the interface so as to align the [001] directions, resulting in a "cube-on-cube" orientation relationship:

$$\mathrm{Al}[001](100) \parallel \mathrm{VN/VC}[001](100). \quad (2)$$

Using this orientation, there is a modest mismatch of 2.3% (3.2%) between the larger VN (VC) ceramic surface unit cell and that of the Al. To accommodate the periodic boundary conditions inherent in a supercell calculation, we invoke the coherent interface approximation [57] in which the (softer) Al is stretched to match the dimensions of the ceramic. In a realistic interface with the above orientation relationship, the mismatch would likely result in an array of widely dispersed misfit dislocations separated by ~180 Å (~129 Å) for the Al/VN (Al/VC) system. Hence, our model mimics the coherent regions between dislocations.

To identify the optimal interface geometry we considered three different stacking sequences, placing the interfacial Al atoms in one of three positions with respect to the ceramic surface lattice structure (see Fig. 4): above the V atoms (V site), above the N/C atoms (N/C site) and along the V–N/C bond direction (bridge site). Adhesion energies were then calculated for each geometry, both before and after allowing for atomic relaxations.

4.2. Work of adhesion

Our estimates of the ideal work of adhesion ($\mathscr{W}_{ad}$) were calculated using two different methods. The first is based on the universal binding energy

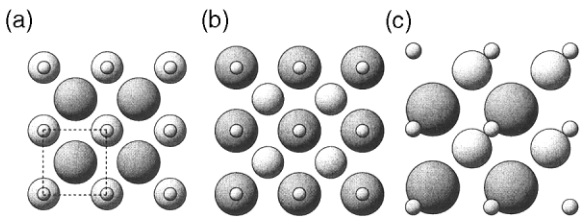

Fig. 4. Three stacking sequences for the Al/VN and Al/VC interfaces. Small spheres, Al interfacial atoms; medium-sized spheres, N/C atoms; large spheres, V atoms. The supercell profile along ⟨100⟩ is shown as a black dotted line. (a) N/C; (b) V; (c) Bridge.

relation (UBER) [58], and involves calculating the total energy of an unrelaxed interface (formed by joining truncated bulk surfaces) as the interfacial separation is incrementally reduced from an initial value of 8 Å. The *ab initio* data are then fit to the UBER function, yielding the optimal $\mathscr{W}_{ad}$ and interfacial separation, d_0 (see Fig. 5). The optimal geometries from the UBER calculations were then used to begin a second series of calculations in which the structure of each interface and its isolated slabs were optimized via minimization of the atomic forces to a tolerance of 0.05 eV/Å. (For those supercells having the V or N/C site stacking, all atomic relaxations were along a direction perpendicular to the interface due to symmetry, and all in-plane forces were equal to zero. Structures

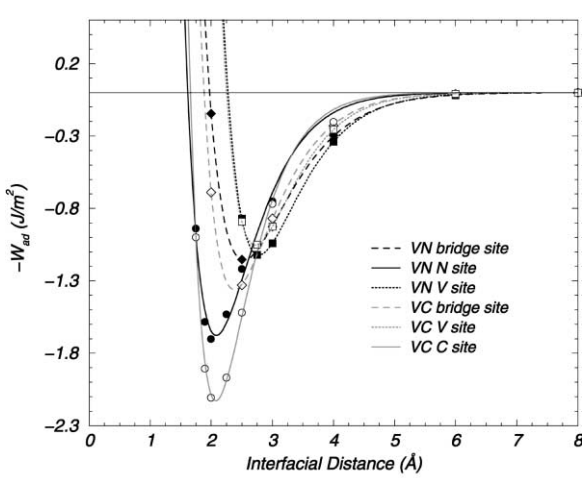

Fig. 5. Universal binding energy curves for the Al/VN and Al/VC interface geometries.

with the bridge-site stacking were constrained to allow relaxations perpendicular to the interface only.) To facilitate cancelation of errors across the different interface models and interface vs. surface calculations, the same supercell dimensions and **k**-points were used whenever possible.

Table 3 summarizes the optimal d_0 and $\mathscr{W}_{ad}$ values for all six interface structures, including both the unrelaxed (UBER) and relaxed geometries. We see that the interfaces with the Al atoms placed above the metalloid atoms exhibit the largest $\mathscr{W}_{ad}$ values for both ceramics: 1.73 J/m^2 for Al/VN and 2.14 J/m^2 for Al/VC. Bonding at the V site is weakest, and is similar (0.91–0.96 J/m^2) for both systems. Intermediate to these two extremes is the bridge site, in which only partial Al–metalloid bonds form. The preference for the metalloid adhesion site is consistent with earlier adhesion studies [59–61] involving interfaces of MgO(100) (which also has the rocksalt structure) with Ti, Ag and Al.

In the LDA–linear combination of atomic orbitals (LCAO) study from Ref. [60], Hong and co-workers noticed that the difference in $\mathscr{W}_{ad}$ between Al/MgO and Ag/MgO correlated with the difference in the surface energies of the metals. This behavior is also evident in the LDA–linear muffin tin orbital (LMTO) results of Schönberger et al., who considered the Ti/MgO and Ag/MgO systems. In the present case we observe the same behavior, only applied to the surface energies of the ceramics. Specifically, the largest $\mathscr{W}_{ad}$ value occurs for the interface containing the ceramic with the largest surface energy: VC. Moreover, the difference in $\mathscr{W}_{ad}$ between the VC and VN interfaces is roughly 0.4 J/m^2, for both the metalloid and bridge sites. This is similar to the difference in ceramic surface energies of 0.32 J/m^2.

The relatively small $\mathscr{W}_{ad}$ values (1.7, 2.1 J/m^2) calculated herein are in reasonable qualitative agreement with those of Refs. [59,60], which range from 2.2 J/m^2 for Ti/MgO down to 1.6–1.9 J/m^2 for Ag/MgO. (However, a direct comparison between these results is not recommended due to differences in computational details such basis sets and exchange-correlation functionals.) The agreement is likely due more to the geometry of the ceramic surfaces rather than the details of the individual

Table 3
Unrelaxed and relaxed adhesion energies ($\mathscr{W}'_{ad}$) and interfacial separations (d_0) for the six Al/VN and Al/VC interface systems

Ceramic	Stacking	Unrelaxed		Relaxed	
		d_0 (Å)	$\mathscr{W}'_{ad}$ (Jm^{-2})	d_0 (Å)	$\mathscr{W}'_{ad}$ (Jm^{-2})
VN	N site	2.08	1.68	2.11	1.73
	V site	2.78	1.12	2.80	0.91
	Bridge	2.53	1.16	2.53	0.98
VC	C site	2.08	2.13	2.13	2.14
	V site	2.72	1.05	2.73	0.96
	Bridge	2.38	1.36	2.31	1.38

metal–ceramic interactions. Namely, the (100) face of rocksalt-type crystals is a non-polar surface with equal numbers of cations and anions within each layer parallel to the interface. The layers are therefore charge neutral, and exhibit smaller surface energies than their polar counterparts. Since smaller surface energies generally indicate a less reactive surface, these non-polar geometries tend to adhere weakly when interfaced with another surface. We have observed similar trends in polar vs. non-polar geometries for other interface systems [7,14], and in a follow-up study will cast this relationship in a more quantitative context [62].

In general, there is good agreement between the unrelaxed UBER and relaxed $\mathscr{W}'_{ad}$ and d_0 values. In allowing for relaxation, interfacial distances change by less than 0.05 Å, and $\mathscr{W}'_{ad}$ is altered by about 0.2 J/m^2 at most. Similar agreement was observed in our earlier study [14] of the Al/WC interface, in which only minor amounts of atomic relaxation were present. However, significant differences between UBER and relaxed $\mathscr{W}'_{ad}$ values have been noted for systems that undergo substantial relaxation [7].

Table 4 shows that allowing for interfacial atomic relaxation results in only small changes to the average interlayer distances (3.5% or less of the respective bulk spacings). In Al, three of the four interlayer distances undergo contraction, presumably in an effort to counteract the lateral tensile strain incurred by matching to the larger ceramic surface cells. In both VN and VC the first interlayer contracts by 0.5%, which is slightly less than what is found for the free surfaces: 1.7% and 1.4%, respectively. However, the degree of rumpling of the ceramic interfacial layer in both systems is nearly identical to that found for the surfaces. In Al/VN the N atom relaxes towards the Al slab, while the V atom contracts slightly deeper into the VN bulk region, resulting in an N–V distance of 0.32 Å. At the surface these atoms are separated by 0.27 Å. In Al/VC the C–N distance is 0.21 Å and in the surface it is 0.18 Å.

Table 4
Interlayer spacing with respect to position perpendicular to the interface, given in terms of absolute distance (Å) and as a percentage of the respective bulk spacing (shown in square brackets). The central layer of the Al slab is denoted Al_3, the interfacial Al layer as Al_1, the central ceramic layer is $Ceramic_4$, etc.

Interlayer	Average interlayer distance (Å) [% of bulk]	
	Al/VN	Al/VC
Al_{2-3}	1.98 [−2.0]	1.95 [−3.5]
Al_{1-2}	2.04 [+1.0]	2.00 [−1.0]
Interface	2.11	2.13
$Ceramic_{1-2}$	2.06 [−0.5]	2.08 [−0.5]
$Ceramic_{2-3}$	2.12 [+2.4]	2.08 [−0.5]
$Ceramic_{3-4}$	2.05 [−1.0]	2.09 [0]

In summary, we find relatively small $\mathscr{W}'_{ad}$ values for both Al/VN and Al/VC interfaces, consistent with the non-polar nature of the rocksalt (100) surface and with earlier studies of metal/MgO adhesion. The magnitude of the difference in $\mathscr{W}'_{ad}$ and its rank-ordering for Al/VN vs. Al/VC can be

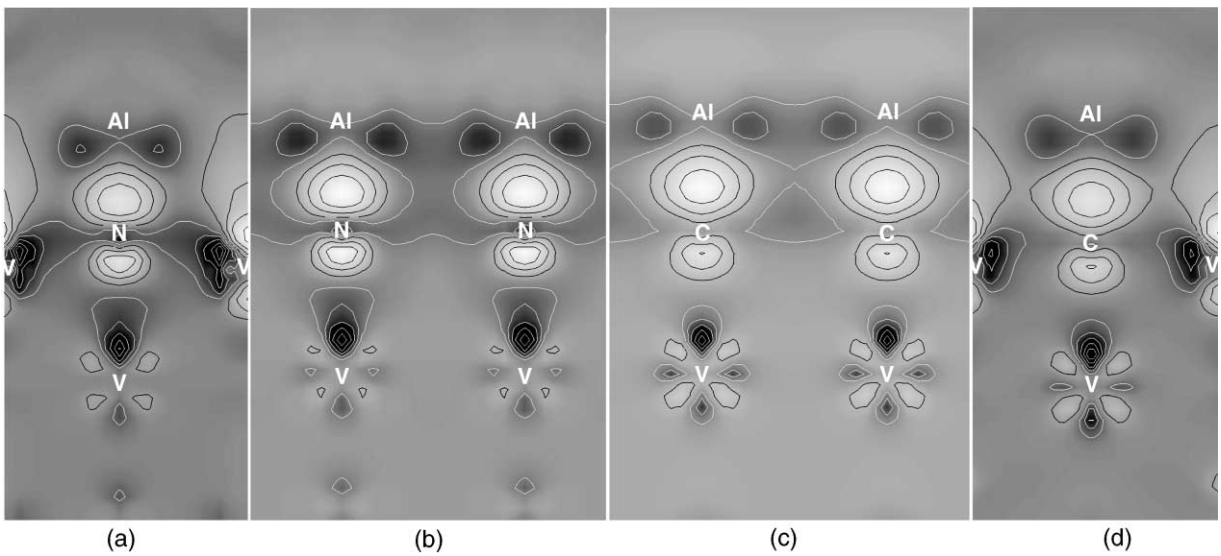

Fig. 6. Charge density difference (relative to the isolated surfaces) for the Al/VN and Al/VC interfaces taken along the (011) and (001) directions. The color scheme is the same as in Fig. 3, and the interfacial atoms intersected by the slice plane are labeled. (a) Al-VN (011); (b) Al-VN (001); (c) Al-VC (001); (d) Al-VC (011).

roughly understood in terms of the differences in the surface energies of the respective ceramics.

4.3. Electronic structure

To reveal the nature of the interfacial bonding between the metal and ceramic, Figs. 6–8 depict the interfacial charge density difference, its planar average along ⟨100⟩ and the layer-projected DOS, respectively, for the relaxed Al/VN and Al/VC interfaces using the optimal metal-on-metalloid stacking sequence. The difference in charge density was evaluated with respect to the isolated slabs according to the relation:

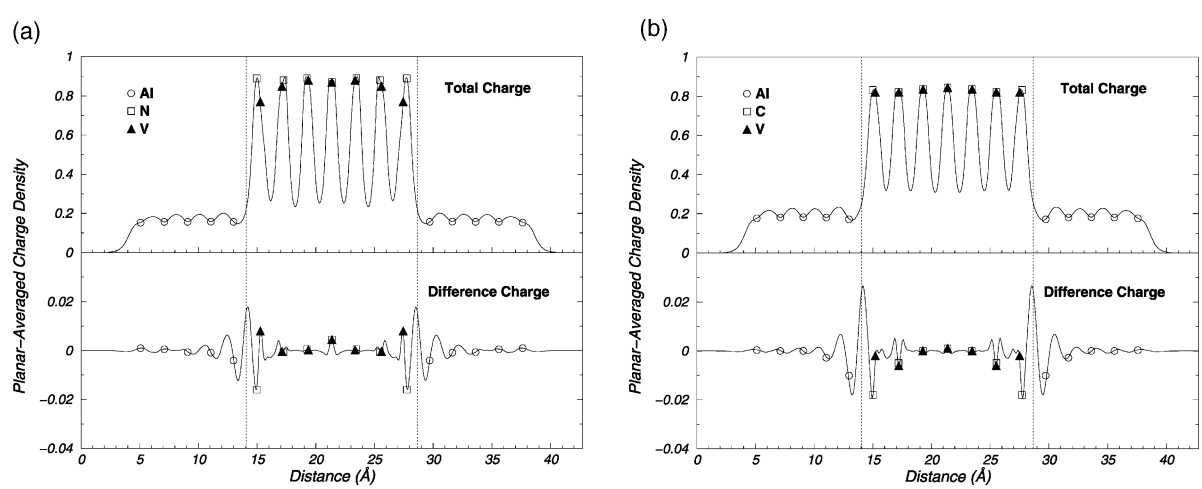

Fig. 7. Planar-averaged total charge and charge density difference (relative to the isolated surfaces) for the Al-above-metalloid geometries along a direction normal to the interfaces. The location of the interfaces is given by dotted vertical lines. (a) Al-VN; (b) Al-VC.

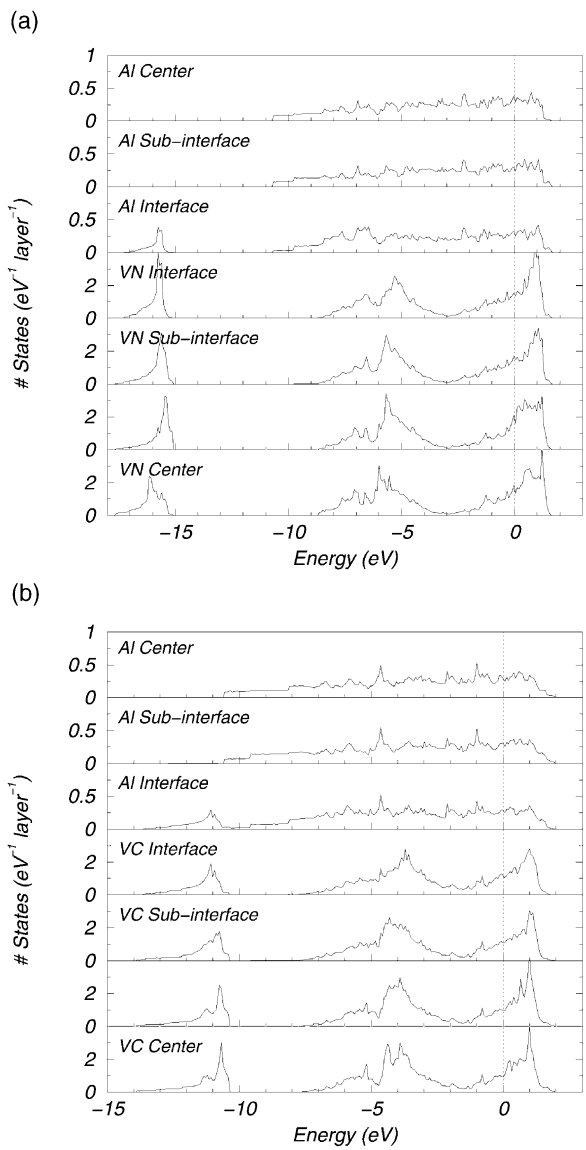

Fig. 8. Layer-projected DOS for the Al/VN and Al/VC interfaces, using the optimal (Al-above-metalloid) stacking sequence. (a) Al-VN; (b) Al-VC.

$$\rho(\boldsymbol{r})_{\text{interface}} - [\rho(\boldsymbol{r})_{\text{Al}(100)} + \rho(\boldsymbol{r})_{\text{VN/VC}(100)}], \tag{3}$$

and is visualized in Fig. 6 with the same gray-scale scheme as used in Fig. 3. Two slices along (011) and (001) are shown for each interface, and those atoms intersected by the slicing planes are identified.

Since the electronic structures of the bulk ceramics are closely related, it should come as no surprise that there are several features of the interfacial electronic structure common to both systems. First of all, Fig. 6 shows that the interfacial charge redistribution is a localized effect, being confined to the first Al layer, and to within the second layer in the ceramics. This conclusion is supported by the DOS plot of Fig. 8, where the sub-interface DOS are similar to their values in the center of their respective slabs. Secondly, there are extended regions of charge depletion in the interstitial regions of the interfacial Al layer, as can be seen both in Fig. 6 and Fig. 7. This signals a reduction in lateral Al–Al metallic bonding in favor of forming new bonds across the interface. Likewise, Fig. 6 shows that lateral bonding in the ceramic interfacial layer also weakens, as seen by the reduction in V *d*-charge in Fig. 6(a) and (d).

The dominant metal–ceramic bonding mechanism appears to be a covalent Al–N (or Al–C) σ-type bond. The bonds can be clearly seen in Fig. 6 as the roughly spherical regions of charge accumulation along the Al–metalloid bond direction. In addition, the lower panels of Fig. 7 show that this charge is peaked slightly closer to the metalloid atom than to the Al, consistent with differences in electronegativity between Al and C/N. The different magnitudes of the planar-averaged charge accumulation at the interface in Fig. 7 also explain the observed differences in magnitude of $\mathscr{W}'_{\text{ad}}$: the larger peak in the Al–C bond charge illustrates that more charge accumulates there than in the weaker Al–N bonds of Al/VN. The DOS from Fig. 8 shows that in Al/VN the bonding is likely due to hybridization of the Al 3*sp* states with the N 2s band in the −17 to −15 eV range. For Al/VC the same type of overlap occurs, except that it now involves the C 2*s* within the −14 to −10 eV range.

To summarize, we find that the dominant interfacial bonding mechanism is the essentially the same for both systems, and involves a covalent Al 3*sp*–N/C 2*s* σ-type interaction. The larger $\mathscr{W}'_{\text{ad}}$ of Al/VC can be explained by the relatively higher charge density (as compared with Al/VN) within the bond orbital.

5. Summary and conclusions

We have performed a GGA–DFT study of the adhesion, structure and bonding of the Al/VN and Al/VC interfaces in order to determine the importance of the ceramic's metalloid component on interfacial properties. We find that for both systems the preferred stacking sequence places the Al atoms above the metalloid sites, consistent with earlier studies of metal/MgO interfaces. W'_{ad} values were calculated to be 1.73 J/m^2 for Al/VN and 2.14 J/m^2 for Al/VC. The larger W'_{ad} value for Al/VC can be attributed to the higher surface energy of VC(100), indicative of a more reactive surface and greater preference for bond formation. In addition, the difference in W'_{ad} was found to be roughly the same size as the difference in the ceramic surface energies, further suggesting a dependence of interfacial properties upon those of its underlying surfaces. An analysis of the interfacial electronic structure revealed that both systems form covalent Al–N/C σ-type bonds. The Al–C bond orbital exhibited a greater concentration of charge, in agreement with that interface's larger W'_{ad}.

Acknowledgements

Computational resources were provided by the National Computational Science Alliance at the University of Illinois at Urbana–Champaign under grant MCA96N001N. Financial support was provided by the National Science Foundation Division of Materials Research under grant DMR9619353. D. Siegel acknowledges General Motors Corporation for financial support during a summer internship.

References

[1] Finnis MW. J Phys: Cond Matter 1996;8:5811.
[2] Lipkin DM, Clarke DR, Evans AG. Acta Mater 1998;46:4835.
[3] Kriese MD, Moody NR, Gerberich WW. Acta Mater 1998;46:6311.
[4] Rice JR. In: Yokobori T, Kawasaki T, Swedlow JL, editors. Proceedings of the 1st International Conference on Fracture, Sendai, Japan, 1966;309–40.
[5] Rao F, Wu R, Freeman AJ. Phys Rev B 1995;51:10052.
[6] Bogicevic A, Jennison DR. Phys Rev Lett 1999;82:799.
[7] Siegel DJ, Hector LG Jr, Adams JB. Phys Rev B, submitted for publication.
[8] Zhang W, Smith JR. Phys Rev Lett 2000;85:3225.
[9] Benedek R, Alavi A, Seidman DN, Wang LH, Muller DA, Woodward C. Phys Rev Lett 2000;84:3362.
[10] Zhukovskii YF, Kotomin EA, Jacobs PWM, Stoneham AM. Phys Rev Lett 2000;84:1256.
[11] Schweinfest R, Köstlmeier S, Ernst F, Elsässer C, Wagner T. Phil Mag A 2001;81:927.
[12] Christensen A, Carter EA. J Chem Phys 2001;114:5816.
[13] Toth LE. Transition metal carbides and nitrides. San Diego (CA): Academic Press, 1971.
[14] Siegel DJ, Hector LG Jr, Adams JB. Surf Sci, accepted for publication.
[15] Hartford J. Phys Rev B 2000;61:2221.
[16] Dudiy SV, Hartford J, Lundqvist BI. Phys Rev Lett 2000;85:1898.
[17] Hohenberg P, Kohn W. Phys Rev 1964;136:864B.
[18] Kohn W, Sham LJ. Phys Rev 1965;140:1133A.
[19] Alemany P. Surf Sci 1994;314:114.
[20] Wenchang L, Kaiming Z, Xide X. Phys Rev B 1992;45:11048.
[21] Li S, Arsenault RJ, Jena P. J Appl Phys 1988;64:6246.
[22] Hoekstra J, Kohyama J. Phys Rev B 1998;57:2334.
[23] Ogata S, Kitagawa H. J Jpn Inst Met 1996;60:1079 (translation from Japanese).
[24] Eustathopoulos N, Nicholas MG, Drevet B. Wettability at high temperatures. Amsterdam: Pergamon, 1999.
[25] Naidich JV. Prog Surf Membr Sci 1981;14:353.
[26] Ramqvist L. Int J Powder Metall 1965;1:2.
[27] Vepřek S. J Vac Sci Technol 1999;15:2401.
[28] Kresse G, Furthmüller J. Phys Rev B 1996;54:11169.
[29] Rappe AM, Rabe KM, Kaxiras E, Joannopoulos JD. Phys Rev B 1990;41:1227.
[30] Kresse G, Hafner J. J Phys: Cond Matter 1994;6:8245.
[31] Press WH, Teukolsky SA, Vetterling WT, Flannery BP. Numerical recipes in Fortran 90: the art of parallel scientific computing, 2nd ed. New York (NY): Cambridge University Press, 1996.
[32] Polak E. Computational methods in optimization. New York: Academic, 1971.
[33] Pulay P. Chem Phys lett 1980;73:393.
[34] Broyden CG. Math Comput 1965;19:577.
[35] Johnson DD. Phys Rev B 1988;38:12087.
[36] Monkhorst HJ, Pack JD. Phys Rev B 1976;13:5188.
[37] Mermin ND. Phys Rev 1965;137:A1441.
[38] Methfessel M, Paxton AT. Phys Rev B 1989;40:3616.
[39] Hellmann H. Einfuhrung in die Quantumchemie. Liepzig: Deuticke, 1937.
[40] Feynman RP. Phys Rev 1939;56:340.
[41] Perdew JP, Chevary JA, Vosko SH, Jackson KA, Pederson MR, Singh DJ. Phys Rev B 1992;46:6671.
[42] Stampfl C, Mannstadt W, Asahi R, Freeman AJ. Phys Rev B 2001;63:155106.

[43] Grossman JC, Mizel A, Côté M, Cohen ML, Louis SG. Phys Rev B 1999;60:6343.
[44] Villars P, Calvert LD, editors. 2nd ed. Pearson's handbook of crystallographic data for intermetallic phases, vol. 2,4. Materials Park (OH): ASM International; 1991.
[45] Häglund J, Grimvall G, Jarlborg T, Guillermet AF. Phys Rev B 1991;43:14400.
[46] Zhukov VP, Gubanov VA. J Phys Chem Solids 1987;48:187.
[47] Zhukov VP, Gubanov VA, Jepsen O, Christensen NE, Andersen OK. J Phys Chem Solids 1988;49:841.
[48] Vanderbilt D. Phys Rev B 1990;41:7892.
[49] Louie SG, Froyen S, Cohen ML. Phys Rev B 1982;26:1738.
[50] Blöchl PE. Phys Rev B 1994;50:17953.
[51] Kresse G, Joubert D. Phys Rev B 1999;59:1758.
[52] Perdew JP, Zunger A. Phys Rev B 1981;23:5048.
[53] Häglund J, Guillermet AF, Grimvall G, Körling M. Phys Rev B 1993;48:11685.
[54] Boettger JC. Phys Rev B 1994;49:16798.
[55] Tyson WR, Miller WA. Surf Sci 1977;62:267.
[56] Tyson WR. Can Metall Quart 1975;14:307.
[57] Benedek R, Seidman DN, Minkoff M, Yang LH, Alavi A. Phys Rev B 1999;60:16094.
[58] Smith JR, Hong T, Srolovitz DJ. Phys Rev Lett 1994;72:4021.
[59] Schönberger U, Andersen OK, Methfessel M. Acta Metall Mater 1992;40:S1.
[60] Hong T, Smith JR, Srolovitz DJ. Acta Metall Mater 1995;43:2721.
[61] Li C, Wu R, Freeman AJ, Fu CL. Phys Rev B 1993;48:8317.
[62] Siegel DJ, Hector LG Jr, Adams JB. Phys Rev Lett, submitted for publication.